Chemical Engineering Science 61 (2006) 835–844

Chemical Engineering Science

www.elsevier.com/locate/ces

Adhesion of solid particles to gas bubbles. Part 2: Experimental

Florin Omota[a], Alexandre C. Dimian[a,*], Alfred Bliek[b]

[a]*Department of Chemical Engineering, University of Amsterdam, Nieuwe Achtergracht 166, 1018 WV Amsterdam, The Netherlands*
[b]*Faculty of Science and Technology, Twente University of Technology, P.O. Box 217, 7500 AE Enschede, The Netherlands*

Received 10 March 2005; received in revised form 16 May 2005; accepted 17 May 2005
Available online 22 September 2005

Abstract

In slurry bubble columns, the adhesion of solid catalyst particles to bubbles may significantly affect the G–L mass transfer and bubble size distribution. This feature may be exploited in design by modifying the hydrophilic or hydrophobic nature of the particles used. Previously we have proposed a generalised model, describing the adhesion of particles to G–L interface under stagnant conditions. In this work, we studied the adhesion of particles characterised by different degree of hydrophobicity and porosity: non-porous polystyrene and glass beads, unmodified and hydrophobised *mesoporous* silica, and activated carbon particles. Images recorded at high optical magnification show the particles adhering to gas bubbles individually or as aggregates. In aqueous media, higher liquid surface tension and particle surface hydrophobicity increase the adhesion strength and the tendency of particles to agglomerate, in agreement with the model. The adhesion of non-porous rough-surface particles to gas bubbles can be characterised by the receding contact angle. The advancing contact angle represents better the adhesion of the same particles to liquid droplets. We found that the "effective" contact angle of porous particles is much lower than an "intrinsic" contact angle calculated from the heat of immersion in water, or measured by sessile drop method. An equivalent contact angle derived from the Cassie rule explains the wetting behaviour of particles having the pores filled with liquid.

Keywords: Catalyst support; Particle; Adhesion; Agglomeration; Bubble; Flotation

1. Introduction

Adhesion of solid particles to bubble is the core mechanism in froth flotation. However, it also plays an important role in antifoaming and in multi phase catalytic reactors. The adhesion of catalyst particles to gas bubbles plays a key role in the enhancement of gas–liquid mass transfer (Ruthiya et al., 2004). Particle-to-bubble adhesion is the result of particle–bubble collisions, adhesive forces and particle detachment due to gravity and shear forces. When a particle and a gas bubble collide, the liquid film between particle and bubble is pinning and a three-phase contact line is formed (Ralston et al., 1999). Subsequently, the particle may remain attached to the gas bubble as result of adhesive forces or may detach due to the action of gravity and/or shear forces. Capillary forces are responsible for particle–bubble stability (Fielden et al., 1996). This work refers to the particle-to-bubble adhesion under stagnant conditions where the detachment probability is minimised.

In earlier work, Omota et al. (2005) proposed a model describing the adhesion of fine particles to a gas bubble. The model explains the influence of particle–particle cohesion strength on particle-to-bubble adhesion. At low cohesion forces, the particles adhere to bubble individually or as monolayer. If the cohesion forces exceed a certain limit, a second layer joins the aggregate. When the cohesion forces are higher than the adhesion forces, the particles form large aggregates adhering to a gas bubble by one or more particles. Hence, the strength of cohesive forces affects the fraction of bubble coverage as well as the maximum weight of particles carried by the bubble.

The objective of the second part is to validate the model using experimental results for the adhesion of particles to a single bubble under stagnant conditions. The models applied in flotation take into account nonporous particles. However,

* Corresponding author. Tel.: +31 20 525 6034; fax: +31 20 525 5604.
E-mail address: alexd@science.uva.nl (A.C. Dimian).

0009-2509/$ - see front matter © 2005 Elsevier Ltd. All rights reserved.
doi:10.1016/j.ces.2005.05.048

in slurry bubble columns, the catalyst particles are highly porous. They might have different behaviour. Therefore, we perform experiments with nonporous and porous particles, characterised by hydrophilic or hydrophobic surfaces.

2. Experimental

2.1. Chemicals

High purity mesoporous silica supplied by Promeks, Batch ID: N58/02, Sample ID G-5268 has a content of minimum 99.95 wt% SiO_2 anhydrous basis. Sieved particles in the range of 35–53 μm were used for particle-to-bubble adhesion experiments and for the preparation of modified silica. Physical properties of unmodified and modified silica particles are given in Table 1. Dichlorodimethylsilane (DDMS), ethanol and isopropanol p.a. from Merck were used without any other treatment.

2.2. Preparation of hydrophobic silica

Ten grams of mesoporous silica was mixed with 87 ml solution containing 30 wt% isopropanol in water. Subsequently, 2.3 ml of DDMS was added under vigorous stirring during 10 min. The suspension was mixed for 30 min at room temperature and then heated up to the boiling point. The vapours were condensed and refluxed for 30 min. After cooling at room temperature, the product was washed with ethanol and bidistilled water. Finally, the powder was dried at 393 K for 16 h.

2.3. Characterisation of silica particles

The specific surface area of modified silica samples was measured by nitrogen adsorption using the BET equation. A Coulter Counter Multisizer 3 System was employed to obtain the particle size distribution. The heat of immersion in water was determined at a constant temperature of 313 K using a Setaram Calvet Calorimeter C80 at a constant temperature of 40 °C. Prior to the micro-calorimetric measurements each sample was pretreated for 3 h at 423 K and 10^{-9} Pa.

2.4. Measurements of three-phase contact angle

The three-phase contact angle was obtained by sessile drop method, using an optical microscope based on Optem X1 objective and Optem Zoom 160, coupled to a high-speed video camera, Photron FASTCAM Ultima SE. The camera offers exceptionally high-speed video recording rates up to 40 500 frames per second (fps) partial frames or 4500 fps full frames at the highest resolution of 256 × 256 pixels. Compressed porous particles absorb the liquid droplet very fast. Therefore, the images were recorded at 4500 fps and analysed by image processing using Matlab v6.5 and Image Processing toolbox v3.1. The contact angle was calculated and represented vs. time.

2.5. Bubble pick-up experiments

Particle to bubble adhesion experiments were carried out in a bubble pick-up (BPU) cell, as described by Wimmers and Fortuin (1988), Vinke et al. (1991a, b), and van der Zon et al. (1999). The cell consists of a holder filled with solid particles, completely immersed in liquid. With the help of a micrometric screw, a small bubble formed at the top of a needle approaches the solid particles in order to pick up particles from the holder. Further, the bubble is retracted a few milimeters above the holder. The cell has two opposite windows, one for image capture and the other for backside illumination. The images recorded with the high speed-video camera were analysed by image processing in Matlab. Video images and video processing allowed us to calculate the particle and bubble size, the bubble coverage angle and the aggregate thickness of particles adhering to gas bubbles.

The microscopic particles were visualised at high optical magnification by using a Mitutoyo 10X objective coupled to an Optem Zoom 160 and a black/white CCD camera Hitachi model KP-M1A. The highest resolution of digital images was 0.5 μm/pixel.

3. Results and discussion

3.1. Particles hydrophobicity

The amount of DDMS varied during the synthesis of hydrophobic particles produces modified silica samples with a variable degree of hydrophobicity. The powder can be easily immersed in water up to 0.23 ml DDMS per gram of mesoporous silica. This means that the contact angle of silica surface remains below of 90°, and the water spontaneously fills the pores. At higher DDMS-to-silica ratio, the water cannot fill the pores, and the average density of particles with air into pores remains lower than the liquid density. The silica particles float at the water surface when the intrinsic contact angle of silica surface becomes higher than 90°. For experiments in aqueous media we used *unmodified* and *modified silica* with a critical ratio of 0.23 ml DDMS/g silica. Therefore, *modified silica* has an intrinsic contact angle of 90°. Table 1 shows some physical properties of unmodified and modified silicas.

The sessile drop is a standard method for measuring the three-phase contact angle of a stagnant liquid drop in contact with a solid surface. If the solid surface consists of compressed hydrophilic powders, the liquid penetrates into the pores and interparticle space. The images recorded by high-speed video at 4500 fps corresponding to a time resolution of 0.22 ms illustrate the spreading and absorption of the liquid on unmodified silica, modified silica and activated carbon.

Table 1
Physical properties of porous particles

Property	Activated carbon[a]	Unmodified silica[b]	Modified silica
BET specific surface area ($m^2\,g^{-1}$)	999	485	514
Heat of immersion in water ($J\,g^{-1}$)	−46	−83	−51
Intrinsic three-phase contact angle (°)	81.2[c]	58[d]	90[d]
Average particle size (μm)	20	44	44
Average pore size (nm)	0.6	8.6	8.4
Pore volume ($cm^3\,g^{-1}$)	0.65	0.98	0.96

[a]Steam-activated peat-based carbon SX1G provided by Norit B.V.
[b]Mesoporous silica provided by Promeks B.V.
[c]Reported by van der Zon et al. (2001).
[d]Based on heat of immersion data and linear equation: $\theta = 134 + 445(\Delta^{\text{imm}} H/A_s)$ with the same units as in the table. The equation is limited to silica particles modified with DDMS.

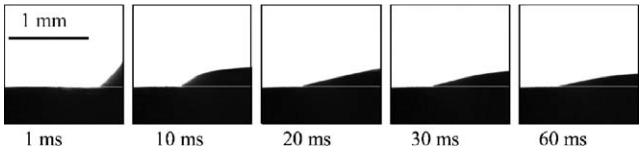

Fig. 1. Dynamic contact angles during spreading and absorption of about 1 μl water on hydrophilic mesoporous silica particles compressed at 1000 bar. Physical properties of silica particles are given in Table 1.

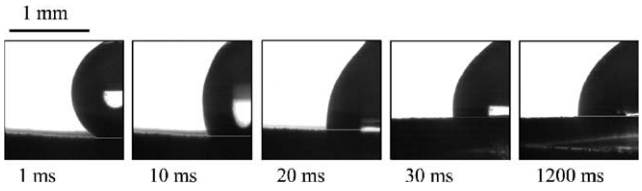

Fig. 2. Dynamic contact angles during spreading and absorption of 1 μl water droplet on hydrophobic mesoporous silica particles compressed at 1000 bar. Physical properties of silica particles are given in Table 1.

A static measurement is impossible for porous particles and thus the contact angle measured is a dynamic contact angle.

Droplets of water with diameters ranging from 1.0 to 1.5 mm were completely absorbed on hydrophilic silica within the first second of contact. The water droplet initially spreads on the surface and a maximum wetted area is reached in about 20 ms. Fig. 1 shows several images recorded during spreading and absorption of a water droplet on a hydrophilic silica disk compressed at 1000 bar. The contact angle measured during the first 10 ms is higher than 30° but decreases in 20 ms to 20°. Ultimately, water is completely absorbed and the dynamic contact angle decreases to zero.

In the case of hydrophobic silica, the water absorption is much slower. Droplets of water spread rapidly in the first 20 ms on the solid surface and then remain stable up to 5 min. Ultimately, water is completely absorbed and the dynamic contact angle decreases again to zero. Fig. 2 shows images recorded during spreading and absorption of a droplet of water on compressed hydrophobic silica. In this case, the advancing contact angle is higher, around 90°, in agreement with the immersion test in water.

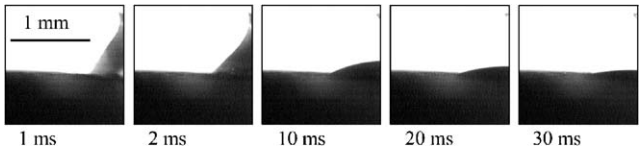

Fig. 3. Dynamic contact angles during spreading and absorption of 1 μl water droplet on activated carbon particles compressed at 1000 bar. Physical properties of activated carbon particles are given in Table 1.

For comparison, the contact angle of a small water droplet was measured on microporous activated carbon particles compressed at 1000 bar. Fig. 3 shows intermediate spreading behaviour between hydrophilic and hydrophobic silica. Initially, the dynamic contact angle is higher than that of the hydrophilic silica. Water is quickly absorbed into the particle interspace and pores, while a dynamic contact angle smaller than 90° is observed, in agreement with other data available in literature. van der Zon et al. (2002) calculated the contact angle of activated carbon $\theta = 81.2°$, using Young's equation and G–L, G–S, and L–G surface tensions.

The water spreading and absorption experiments allow us to measure the advancing contact angle of hydrophilic and moderately hydrophobic porous particles. Compared to contact angles measured by the sessile drop method on flat and smooth surfaces, these results are influenced by the porosity, particle size, compression pressure and time. Therefore, the contact angle of compressed powders may differ from that of a single solid particle adhering to a gas bubble.

During water absorption into pores and interparticle voids, the dynamic contact angle decreases quickly for hydrophilic but slowly for hydrophobic porous powders, until the liquid is completely absorbed. A receding contact angle cannot be measured, but is probably very close to zero. Hydrophilic porous particles in contact with saturated vapours of water must have the pores completely filled with liquid due to capillary condensation. Thus, the solid surface is partially

Table 2
Non porous spherical particles used in bubble pick up experiments

Solid nature	Size (μm)
Hydrophilic glass beads	110–180
Hydrophobic glass beads	110–180
Polystyrene	200–250

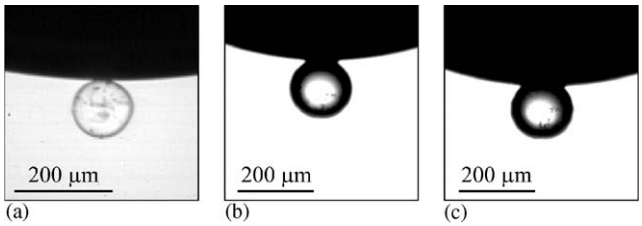

Fig. 4. Nonporous particles adhering to air bubbles: (a) hydrophilic glass bead in α-methyl styrene, $d_p = 126$ mm, $d_b = 2.2$ mm, $\varphi = 6.4°$, $\theta = 7.4°$; (b) hydrophilic glass bead in water, $d_p = 165$ mm, $d_b = 1.3$ mm, $\varphi = 17.5°$, $\theta = 20°$; (c) hydrophobic glass bead in water $d_p = 165$ mm, $d_b = 1.3$ mm, $\varphi = 34.8°$, $\theta = 39°$.

covered with droplets of water and becomes more hydrophilic than a dry surface.

3.2. Adhesion of a single particle to a gas bubble

3.2.1. Nonporous spherical particles

Particle-to-bubble adhesion experiments were performed with particles of different nature, size and porosity. Table 1 depicts the physical properties of porous particles, while Table 2 illustrates the size of non-porous particles. Fig. 4a shows a spherical glass bead adhering to an air bubble in α-methyl styrene (AMS). After extensive silylation with DDMS, the glass surface becomes hydrophobic in water but lyophilic in AMS. Under stagnant conditions silylated glass beads do not adhere to air bubbles in AMS.

Figs. 4b and c show hydrophilic and hydrophobic glass beads in water adhering to air bubbles. The difference between these images consists of different penetration angle of the particles and different contact angles at the three-phase contact line. In water, the penetration angle of hydrophobised glass beads is higher than of hydrophilic ones. Omota et al. (2005) demonstrated that surface hydrophobicity increases the penetration angle of a single particle, when the other properties remain constant. A particle showing low penetration angle can be easier detached because the three-phase contact line is shorter and the orientation of capillary forces is less favourable for adhesion.

The penetration angle of hydrophilic glass beads is smaller in AMS than in water (Figs. 4 a and b) due to a lower contact angle, lower liquid density, and lower liquid surface tension. Among these parameters, the contact angle remains the most important parameter. Table 3 illustrates the influence of the contact angle and penetration angle on the maximum adhesion force.

The particles with smooth surfaces have a single equilibrium position. Surface heterogeneity leads to a hysteresis phenomenon of the contact angle. Figs. 5a and b shows the three-phase contact angles of a polystyrene particle adhering to an air bubble in water, and a polystyrene particle adhering to a droplet of water in air, respectively. The contact angles are different, most probably due to the surface roughness. The receding and advancing contact angles of water on polystyrene reported by Adão et al. (1998) are 46°and 96°, respectively. Craig et al. (1960) reported a receding contact angle of 64°and an advancing contact angle of 86°. In Figs. 5a and b the polystyrene particles show similar contact angles, of 41°and 91°. It appears that the contact angle of a particle adhering to a gas bubble is closer to the receding contact angle, while the contact angle of a particle adhering to a droplet of liquid is similar to the advancing contact angle. When a particle is approaching from the liquid side to the G–L interface, the liquid film between particle–bubble is pinning. The dewetting of solid surface takes place according to a receding contact angle. Therefore, the penetration angle observed experimentally depends on the dewetting process and final area of dry solid surface.

3.2.2. Porous particles

Theoretically, hydrophilic particles can adhere to gas bubble if they are sufficiently small and the contact angle is non-negative (Omota et al., 2005). By decreasing the particle size, the capillary forces become dominant. In this case, the model predicts an equilibrium penetration angle φ almost equal to the contact angle θ. For example, an air bubble with radius $R_b = 0.5$ mm is expected to be completely covered with a monolayer of particles when the particle radius $R_p = 20$ μm and the contact angle is higher than 4°. Irrespective of the surface hydrophobicity, mesoporous silica particles with an average size of 44 μm adhere to gas bubbles.

Fig. 6 shows two particles adhering to air bubbles in water. A hydrophilic particle (case a) shows a penetration angle of about 30°, while a hydrophobic particle (case b) shows a penetration angle of 38°. In contrast to spherical nonporous particles, measuring the penetration angle is not accurate due to irregular shape. However, the difference between the penetration angles of hydrophilic and hydrophobic porous particles is less pronounced and smaller than in the case of nonporous glass beads shown in Figs. 4b and c.

The wetting properties of a surface of porous material filled with liquid are different compared to a smooth surface. Adopting the Cassie and Baxter (1944) approach, an effective three-phase contact angle between the gas, liquid and partially wetted surface is

$$\cos\theta_{\text{ef}} = p\ \cos\ \theta_L + (1 - p)\cos\theta_S, \tag{1}$$

where p is the fraction of surface covered with liquid, θ_L the contact angle of wetting liquid and θ_S the intrinsic contact angle of solid. The liquid spontaneously wets the pores'

Table 3
Characteristics of spherical nonporous particles adhering to air bubbles under stagnant conditions

Solid and liquid nature	Contact angle θ^a (°)	Penetration angle φ^a (°)	$F_{adh,max}{}^b$ (10^{-9} N)	$N_T{}^c$
Hydrophilic glass in AMS	7	6	34	3
Hydrophilic glass in water	20	17	956	29
Hydrophobic glass in water	39	35	3657	106
Polystyrene in water	41	36	5255	6197

[a]Measured.
[b]Calculated.
[c]Estimation of the maximum number of particles of an aggregate capable to adhere to an air bubble through a single particle.

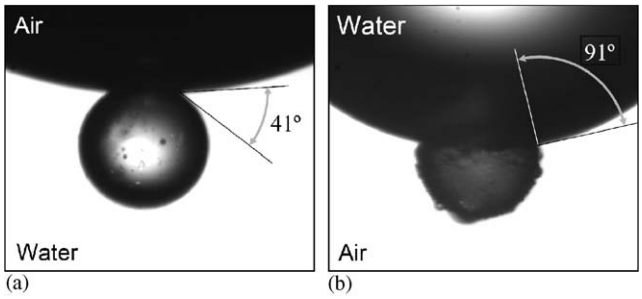

Fig. 5. Adhesion of a polystyrene particle to gas–liquid interface showing different contact angles: (a) air bubble in water $d_b = 1.61$ mm, $d_p = 0.215$ mm, and (b) water droplet in air $d_d = 0.94$ mm, $d_p = 0.205$ mm.

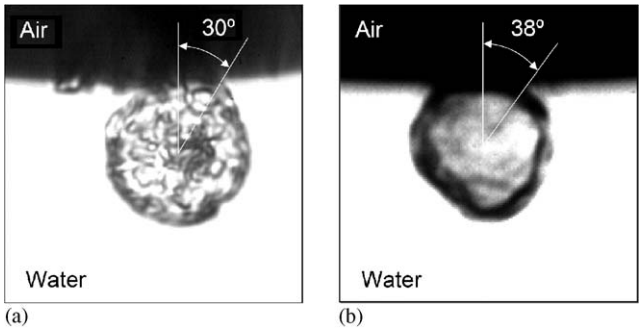

Fig. 6. Mesoporous silica particles $d_p = 44\,\mu$m adhering to air bubbles $d_b = 1$ mm in water: (a) hydrophilic particle, and (b) hydrophobic particle. Physical properties of silica particles are given in Table 1. Due to the irregular particle shape, the penetration angles are only roughly estimated.

area, θ_L being zero. The effective contact angle θ_{ef} will be always smaller than θ_S. A similar approach explains a higher effective contact angle of hydrophobic rough surfaces. The liquid do not wet completely the solid surface entrapping micro bubbles. Similarly for $\theta_S > 90°$ one gets an effective contact angle $\theta_{ef} > \theta_S$.

An aggregate of nonporous, spherical and smooth particles characterised by a well-defined contact angle can be represented by a porous particle as shown in Figs. 7a and b. The adhesion to the gas bubble takes place through a single or only few particles, much smaller than the aggregate size. The capillary force of a spherical particle increases with R_p and $\sin^2(\theta/2)$. Hence, the same capillary force of small particles with large contact angles or larger particles

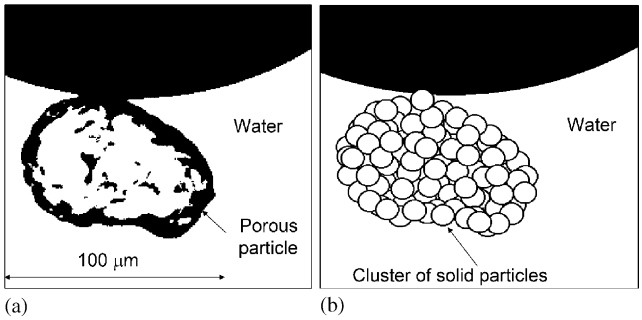

Fig. 7. Image of an unmodified mesoporous silica particle $d_p = 76\,\mu$m adhering to an air bubble $d_b = 368\,\mu$m in water (a) and drawing of an aggregate of particles adhering to a gas bubble (b). Physical properties of silica particles are given in Table 1.

with lower contact angles may be equal. A single porous particle with pores filled with liquid has similar behaviour as an aggregate of non-porous particle adhering through a single particle. The effective contact angle of aggregate is thus smaller than the intrinsic contact angle on nonporous particles.

3.3. Adhesion of particles to a gas bubble as monolayer

3.3.1. Hydrophilic silica

In the pick-up cell, hydrophilic mesoporous silica particles with an average size of 44 μm adhere to air bubbles in water only as monolayer (Figs. 8a and b). When reducing the bubble size, some particles detach from the bubble's bottom. Thus, the number of particles adhering to gas bubble decrease, but the coverage angle increase, in agreement with the behaviour predicted by the model. Fig. 9 shows the bubble coverage angle vs. bubble size, the model and experimental data showing the same trend.

The particle-to-bubble model correlates the three-phase contact angle with bubble coverage angle and bubble size. Thus, the contact angle can be calculated, as proposed by Vinke et al. (1991a,b). The contact angle of hydrophilic particles estimated by modelling particle-to-bubble adhesion is much less than obtained by direct measurements. For Pd/C catalyst particles adhering to hydrogen bubbles in water, Vinke et al. (1991a, b) found a contact angle $\theta = 2.2°$.

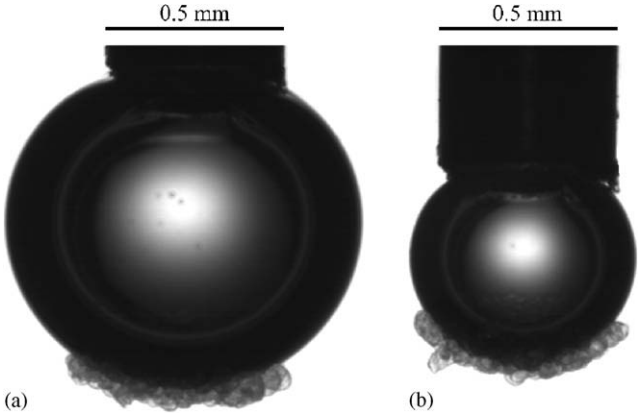

Fig. 8. Image of unmodified mesoporous silica particles adhering to a large (a) and small (b) air bubble. Physical properties of silica particles are given in Table 1.

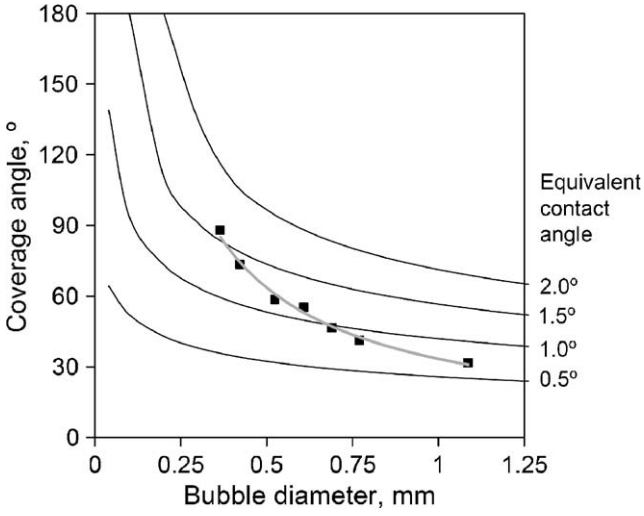

Fig. 9. Influence of bubble diameter on the coverage angle measured experimentally for hydrophilic mesoporous silica particles and calculated by modeling at different contact angles. Physical properties of silica particles are given in Table 1.

Table 4 shows the adhesion forces, equivalent number of particles in an aggregate, and the contact angles calculated by applying the model to the smallest and the largest bubble. These results indicate low contact angles and low adhesive forces of porous hydrophilic particles adhering to air bubbles in water.

The coverage angle increase by decreasing the bubble size. The experimental data shows sharper influence than predicted by the model. Several explanations may be given. Firstly, the attachment probability of particles to large bubbles is lower than to small bubbles. Secondly, the detachment probability of a particle increases as the bubble size and the number of particles. Thirdly, the bubble shape varies with the bubble size. Small bubbles remain almost spherical due to low solid loading and high curvature of the G–L interface. In contrast, large bubbles change their shape easier by retaining more solid particles. If a bubble elongates in vertical direction, the tangential forces on adhering particles increase and consequently, the coverage angle decreases.

3.3.2. Hydrophobic particles

Hydrophobic silica and activated carbon particles form agglomerates in water. Therefore, it is difficult to pick-up only a monolayer. van der Zon et al. (1999) illustrated the formation of large Pd/C aggregates in water but smaller in methyl acrylate/water mixtures. Therefore, we studied the adhesion and agglomeration behaviour by performing experiments in mixtures of water/ethanol at different concentrations. Hydrophobic silica particles do not agglomerate at all when the concentration of ethanol increases to 10 wt%. At this concentration, the particles adhere to gas bubbles only as monolayer, as can be seen in Fig. 10.

By increasing the concentration of ethanol up to 90 wt%, the adhesion forces drop to zero and the particles do not adhere to air bubbles. Wimmers and Fortuin (1988) discussed the adhesive properties of 10 wt% Pd/C and 10 wt% Pd/Al_2O_3 to hydrogen bubbles in ethanol/water solutions. Despite the difference in the support hydrophobicity, they found for both catalysts a linear increase of the coverage angle with the liquid surface tension. However, in aqueous media Pd/C shows a stronger adhesion to hydrogen bubbles than Pd/Al_2O_3, while opposite is true at higher ethanol concentration.

Zisman (1964) found an empirical linear relation between the cosine of the contact angle and the liquid surface tension of the sessile drop. The so-called “critical wetting tension” is reached when the contact angle drops to zero for mixtures. For example, adding ethanol to water lowers both the superficial tension and the three-phase contact angle. By consequence, the adhesive forces of particles to gas bubbles reduce too. Therefore, the critical wetting tension explains why solid particles do not adhere to gas bubbles in liquids with low surface tension.

In Fig. 10a, the image of a bubble covered with a monolayer of hydrophobic silica particles demonstrates strong adhesion forces between particles and bubble, and weak cohesion forces between particles. Compared with similar but hydrophilic particles, the bubble coverage is higher at the same bubble size. Fig. 10b shows relatively low packing of particles covering the upper part of an air bubble. Since the particles have a slight tendency to agglomerate, some voids are present in the structure. Weak cohesive forces between particles keep the structure stable under stagnant conditions but may not be strong enough under shear forces (Roizard et al., 1999). The tangential forces make particles packing higher at the bottom of bubbles. Under dynamic conditions, the aggregate structure adopts a more stable conformation resulting in higher particle packing and lower bubble coverage.

Table 4
Characteristics of porous particles adhering to air bubbles under stagnant conditions

Solid particles	Liquid	Bubble radius R_b (μm)	Coverage angle $\alpha^{(\circ)}$	Aggregate thickness h_T (μm)	$F_{adh,max}$[a] (10^{-9} N)	N_T[b]	$F_{coh,max}$[c] (10^{-9} N)	Contact angle θ^d (°)
Unmodified silica, $R_p = 22\,\mu m$	Water	182	88	Monolayer	1.9	11	—	1.6
		543	32	Monolayer	0.37	2	—	0.7
Modified silica[e], $R_p = 22\,\mu m$	10 wt% ethanol solution in water	360	117	Monolayer	5.4	34	—	2.7
		475	68	Monolayer	2.4	15	—	1.8
Modified silica[e], $R_p = 22\,\mu m$	Water	299	180	65	15.9	97	7.9	4.6
		600	45	66	2.7	17	1.4	1.9
Activated carbon, $R_p = 10\,\mu m$	Water	300	180	63	8.4	542	5.9	5.0
		429	91	55	4.6	299	2.8	3.7

[a]Calculated for monolayer or multilayer adhesion.
[b]Estimation of maximum number of particles of an aggregate adhering to an air bubble through a single particle.
[c]Negligible for monolayer; calculated for multilayer adhesion.
[d]Equivalent contact angle of a nonporous spherical particle with the same ρ_S and R_p.
[e]Intrinsic contact angle equal to 90°.

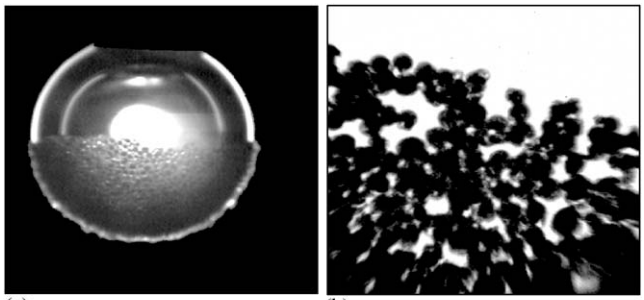

Fig. 10. Image of a small air bubble covered with modified silica particles in ethanol/water solution at 293 K (a) and detail of the upper part of monolayer; (b) showing particle distribution at the bubble surface: $R_p = 22\,\mu m$, $\theta = 90°$, $R_b = 0.55\,mm$, and $c_{ethanol} = 10\,wt\%$. Physical properties of silica particles are given in Table 1.

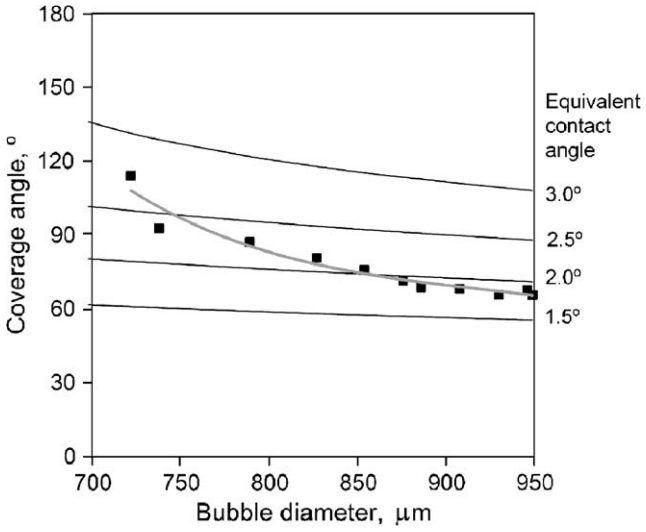

Fig. 11. Influence of bubble diameter on the coverage angle measured experimentally for modified mesoporous silica particles and calculated by modeling at different contact angles. Physical properties of silica particles are given in Table 1.

Table 4 shows maximum adhesion forces calculated from the coverage angles for various bubble sizes. The effective contact angles calculated from the adhesion forces are in the range of 1.8–2.7°. These values are significantly lower than the intrinsic contact angle, 90°. As a result, the adhesion forces of porous particles are lower than the adhesion forces of non-porous particles characterised by the same intrinsic contact angle.

Fig. 11 shows the influence of bubble size on the coverage angle. The hydrophobic particles have the same trend as hydrophilic particles. Compared with similar hydrophilic particles, the contact angles are about 2.5 times higher. Both the model and experimental data show that by increasing the surface hydrophobicity both the contact angle and bubble coverage angle increase.

3.4. Multilayer adhesion of particles to a gas bubble

In water, small hydrophobic particles agglomerate and form aggregates. Under stagnant conditions, a bubble kept into a suspension of hydrophobic particles may capture at the G–L interface both individual particles and aggregates. The layer of particles adhering to bubbles has an almost constant thickness exceeds several times the particle size. The adhesion behaviour of hydrophobic mesoporous silica particles and activated carbon particles are further compared.

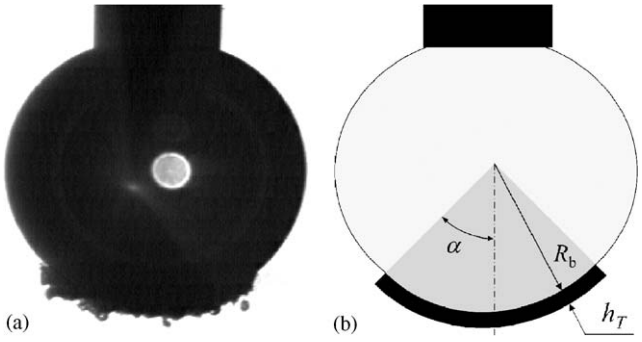

Fig. 12. Image of an air bubble partially covered with modified silica particles in ethanol/water solution at 293 K (a) and drawing of corresponding multilayer of particles; (b) $R_p = 17\,\mu m$, $R_b = 0.6\,mm$, $c_{ethanol} = 10\,wt\%$, and $d = 66\,\mu m$. Physical properties of silica particles are given in Table 1.

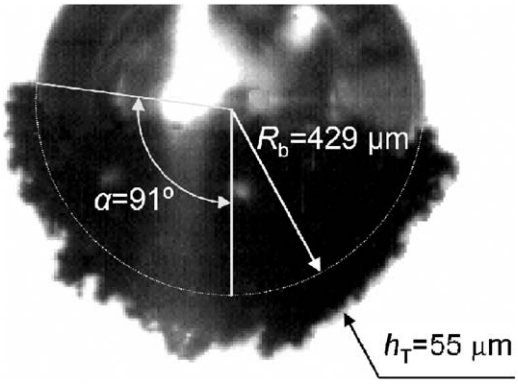

Fig. 13. Image of an air bubble covered with activated carbon particles, $R_p = 10\,\mu m$. Physical properties of activated carbon particles are given in Table 1.

3.4.1. Hydrophobic silica particles

Fig. 12a shows the image of a small air bubble covered with a multi-layer of hydrophobic silica particles. The particles are uniformly distributed at the bubble's bottom. Aggregate thickness corresponds to about two layers of particles. Fig. 12b illustrates the main model parameters describing the multilayer adhesion. The sediment volume in water V_{sed} of a certain mass m of dry solid particles gives the fraction of solid particles as follows:

$$\varepsilon_S = \frac{m(1 + P_v \rho_L)}{V_{sed} \rho_S}. \quad (2)$$

From experiments, a value of $\varepsilon_S = 0.55$ is obtained. Table 4 shows the maximum adhesion force and maximum cohesion force calculated from the model and experiments. An estimate of the contact angle in water yields higher values than in 10 wt% ethanol solution. As in the case of monolayer adhesion, the effective contact angles are much lower than those calculated from contact angle measurements by the sessile drop method.

3.4.2. Hydrophobic activated carbon particles

As in the case of hydrophobic silica, activated carbon particles adhere to air bubble mainly as multilayer as shown in Fig. 13. The average thickness of aggregate adhering to bubble is about three times higher compared with the particle size. Table 4 shows adhesion and cohesion forces lower than hydrophobic silica, mainly because of smaller particle size. The effective contact angles calculated from bubble coverage angle and aggregate thickness are slightly higher than previous values, demonstrating high adhesion and cohesion strength.

Activated carbon particles have irregular shapes compared with almost spherical silica particles. This results in a non-uniform thickness of the aggregate adhering to air bubble. van der Zon et al. (2001) showed that activated carbon particles adhering to nitrogen bubbles in water form large beads, while the same particles adhering to hydrogen bubbles in water have low tendency to agglomerate.

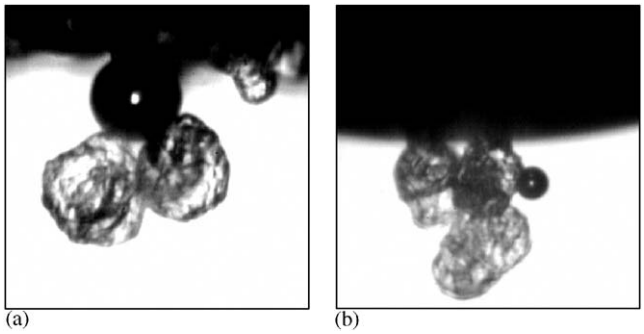

Fig. 14. Complex aggregates of modified mesoporous silica particles and air microbubbles in water: (a) two particles R_p(left) = 25 µm and R_p(right) = 22 µm, adhering to a microbubble $R_b = 21\,\mu m$; (b) micro bubble $R_b = 7.4\,\mu m$ attached to an aggregate of particles. Physical properties of silica particles are given in Table 1.

3.5. Complex aggregates

The theory described here and the experiments performed in bubble pick up cell under stagnant conditions show that the particles immersed in liquid can adhere to the gas bubbles. On the other hand, we found micro bubbles adhering to solid particles as observable in Figs. 14a and b. Small bubbles can be formed when hydrophobic particles are immersed in water or during bubble break-up. In slurry reactors, micro bubbles adhering to solid catalyst particles might explain an enhancement of the reaction rate. The micro bubble acts as a gas reservoir increasing gas concentration in liquid phase, close to the catalyst particle.

The interactions between particles and micro bubbles in dynamic systems may result in complex aggregates. Such aggregates might have an overall density equal with liquid density, zero rise velocity and thus an indefinite residence time. The stability of such heterogeneous aggregates can be explained by attractive van der Waals forces between particle and particle, but also by capillary forces between micro bubble and adjacent particles.

4. Conclusions

The paper presents experiments regarding the adhesion of small particles to gas bubbles under stagnant conditions. The experiments handle the adhesion of: (i) a single spherical particle, (ii) a monolayer of particles, and (iii) an aggregate of particles.

Both the cohesion and adhesion forces increase by higher surface hydrophobicity. Accordingly, hydrophilic particles adhere to bubbles individually or as monolayer, while hydrophobic particles adhere as multilayer.

The contact angle of porous particles adhering to bubbles is much lower than the intrinsic contact angle calculated from the heat of immersion in water or advanced contact angle measured by sessile drop method. According to Cassie and Baxter (1944) approach applied to particles with pores filled with liquid, the effective three-phase contact angle between the gas, liquid and partially wetted surface is lower than the intrinsic contact angle. As a result, the adhesion forces of porous particles are lower than that of non-porous particles.

Particle-to-bubble adhesion of porous particles, as those frequently used in three-phase reactors, is therefore significantly less than that observed for nonporous solids encountered in mineral flotation.

With respect to the industrial application, this work demonstrates that enhancing the hydrophobicity of catalyst solid particles may contribute to getting higher bubble coverage and higher mass transfer in slurry reactors. However, the results are limited to dispersions of particles with narrow size distribution and small bubbles up to 1.5 mm in diameter limited by bubble stability reasons.

Notation

A_s	specific surface area, $m^2\,g^{-1}$
d	diameter, assuming spherical shape, m
$F_{adh,max}$	maximum adhesion force of a particle adhering to a gas bubble, N
h_T	thickness of particle aggregate in multilayer adhesion, m
$\Delta^{imm}H$	heat of immersion in water, $J\,g^{-1}$
m	mass of dry solid particles, kg
N_T	number of particles in an aggregate adhering to bubble through a single particle
p	the fraction of external particle surface covered with liquid
P_v	specific pore volume, $m^3\,kg^{-1}$
R	radius, assuming spherical shape, m
V_{sed}	volume of sediment, m^3

Greek letters

α	coverage angle defined as the angle formed by the centre of a particle, the centre of a spherical bubble, and the lowest pole of the bubble, in vertical plane, rad
ε_S	volumetric fraction of particles including their pores
θ	three-phase contact angle for a single particle adhering at the G–L interface, rad
ρ_L	liquid density, $kg\,m^{-3}$
ρ_S	density of porous particles having the pores filled with liquid, $kg\,m^{-3}$
φ	angle of penetration of a particle into the G–L interface, rad

Subscripts

b	bubble
L	liquid
p	particle
S	solid

Acknowledgements

This research is supported by the Technology Foundation STW, applied science division of NWO and the technology program of the Ministry of Economic Affairs. The authors also gratefully acknowledge Akzo-Nobel, DSM Research B.V., Shell Global Solutions, Engelhard B.V., Promeks ASA, Norit B.V. and Sasol for their financial support.

References

Adão, M.H., Fernandes, A.C., Saramago, B., Cazabat, A.M., 1998. Influence of preparation method on the surface topography and wetting properties of polystyrene films. Colloids and Surfaces A: Physicochemical and Engineering Aspects 132, 181–192.

Cassie, A.B.D., Baxter, S., 1944. Wettability of porous surfaces. Transactions of the Faraday Society 40, 546–551.

Craig, R.G., Berry, G.C., Peyton, F.A., 1960. Wetting of poly-(methyl methacrylate) and polystyrene by water and saliva. Journal of Physical Chemistry 64 (5), 541–543.

Fielden, M.L., Hayes, R.A., Ralston, J., 1996. Surface and capillary forces affecting air bubble–particle interactions in aqueous electrolyte. Langmuir 12, 3721–3727.

Omota, F., Dimian, A.C., Bliek, A., 2005. Adhesion of solid particles to a gas bubble. Part 1: modelling. Chemical Engineering Science, this issue, doi:10.1016/j.ces.2005.07.005.

Ralston, J., Fornasiero, D., Hayes, R., 1999. Bubble–particle attachment and detachment in flotation. International Journal of Mineral Processing 56, 133–164.

Roizard, C., Poncin, S., Lapicque, F., Py, X., Midoux, N., 1999. Behavior of fine particles in the vicinity of a gas bubble in a stagnant and a moving fluid. Chemical Engineering Science 54, 2317–2323.

Ruthiya, K.C., van der Schaaf, J., Kuster, B.F.M., Schouten, J.C., 2004. Modeling the effect of particle-to-bubble adhesion on mass transport and reaction rate in a stirred slurry reactor: influence of catalyst support. Chemical Engineering Science 59, 5551–5558.

Vinke, H., Hamersma, P.J., Fortuin, J.M.H., 1991a. Particle-to-bubble adhesion in gas/liquid/solid slurries. A.I.Ch.E. Journal 37, 1801–1809.

Vinke, H., Bierman, G., Hamersma, P.J., Fortuin, J.M.H., 1991b. Adhesion of small particles to gas bubbles: determination of small effective solid–liquid–gas contact angles. Chemical Engineering Science 46, 2497–2506.

Wimmers, O.J., Fortuin, J.M.H., 1988. The use of adhesion of catalyst particles to gas bubbles to achieve enhancement of gas adsorption in slurry reactors I-. Investigation of particle-to-bubble adhesion using the bubble pick-up method. Chemical Engineering Science 43, 303–312.

Zisman, W.A., 1964. Relation of equilibrium contact angle to liquid and solid constitution. Advances in Chemistry Series 43, 1–51.

van der Zon, M., Hamersma, P.J., Poels, E.K., Bliek, A., 1999. Gas–solid adhesion and solid–solid agglomeration of carbon supported catalysts in three-phase slurry reactors. Catalysis Today 48, 131–138.

van der Zon, M., Thoolen, H., Hamersma, P.J., Poels, E.K., Bliek, A., 2001. Agglomeration and adhesion of catalyst particles in gas–liquid reactors. Catalysis Today 66, 263–270.

van der Zon, M., Hamersma, P.J., Poels, E.K., Bliek, A., 2002. Coalescence of freely moving bubbles in water by the action of suspended hydrophobic particles. Chemical Engineering Science 57, 4845–4853.